



HAL
open science

Structural Transformations in Medium- and High-Entropy Alloy Systems in Course of High-Energy Ball Milling

A. Rogachev, D. Kovalev, A. Fourmont, S. Vadchenko, N. Kochetov, N. Shkodich, Florence Baras, O. Politano, D. Moskovskikh

► **To cite this version:**

A. Rogachev, D. Kovalev, A. Fourmont, S. Vadchenko, N. Kochetov, et al.. Structural Transformations in Medium- and High-Entropy Alloy Systems in Course of High-Energy Ball Milling. International Journal of Self-Propagating High Temperature Synthesis, 2022, 31 (2), pp.62-68. 10.3103/S1061386222020078 . hal-03851494

HAL Id: hal-03851494

<https://hal.science/hal-03851494>

Submitted on 15 Nov 2022

HAL is a multi-disciplinary open access archive for the deposit and dissemination of scientific research documents, whether they are published or not. The documents may come from teaching and research institutions in France or abroad, or from public or private research centers.

L'archive ouverte pluridisciplinaire **HAL**, est destinée au dépôt et à la diffusion de documents scientifiques de niveau recherche, publiés ou non, émanant des établissements d'enseignement et de recherche français ou étrangers, des laboratoires publics ou privés.

Structural transformations in medium- and high-entropy alloy systems in course of high-energy ball-milling

Alexander Rogachev ^{a,*}, Dmitry Kovalev ^a, Adrien Fourmont^b, Sergei Vadchenko^a, Nikolas Kochetov^a, Natalia Shkodich^a, Florence Baras^b, Olivier Politano^b and Dmitry Moskovskikh^c

^a*Merzhanov Institute of Structural Macrokinetics and Materials Science, Russian Academy of Sciences, Chernogolovka, 142432 Russia;*

^b*ICB laboratory, UMR 6303 CNRS-Université Bourgogne Franche-Comté, 9 Av. Alain Savary, BP 47870, 21078 Dijon Cedex, France;*

^c*Center of Functional Nanoceramics, National University of Science and Technology MISiS, Moscow, 119049, Russia.*

* *Corresponding author.*

E-mail address: rogachev@ism.ac.ru

Abstract

Dynamics of medium- and high-entropy phases formation during the process of mechanical alloying by means of high-energy ball milling (HEBM) are studied for the equimolar CoCrFeNi, AlCoCrFeNi, and CoCrFeMnNi alloys. Using step-by-step X-ray diffraction analysis, it is found that a specific structural transformation occurs after some critical time of HEBM. It is suggested that this transformation converts nanocrystalline intermediate solid solutions, formed due to severe plastic deformation during HEBM, into single-phase multicomponent alloys in relatively short period of time.

Keywords: high-entropy alloys; high-energy ball-milling; mechanical alloying; crystal structure; X-ray diffraction

1. Introduction

Nanostructured multiple principal elements alloys (MPEAs) [1], also known as high entropy alloys (HEAs) [2], induced a breakthrough in alloys production [3–6]. These novel materials consist of five or more components taken in comparable or even equal amounts. High-entropy alloys obtained by mechanical alloying in planetary ball mills mostly belongs to the family of 3d transition metals [7–13]. Firstly, nanocrystalline six-component solid solution AlCoCrCuFeNi was obtained after 42-60 hours of ball milling [7]. The system AlCoCrFeNi remains in a focus of research [8–10], as well as Cantor alloy CoCrFeMnNi [11–13]. All these alloys have a four-component core, composed of 3d-transition metals

Co, Cr, Fe, and Ni. Fifth elements such as Al or Mn also can serve as constituting components in this transition metals HEAs family. Presence of Fe and Cr as major components brings to naught possible influence of the milled powders contamination with these elements from steel milling drum and balls, as a result of intense friction. Using of high-energy planetary ball mills allowed significant shortening time of mechanical alloying, - from dozens of hours down to dozens of minutes [9,10,13]. Despite extensive research, the dynamics of HEAs formation during HEBM has not been adequately described yet. It is generally accepted that a mutual interdiffusion of metallic components should play leading role in the formation of complex solid solutions; nevertheless, the mechanism and kinetics of this process remain obscure. Some recent experimental results and analysis of available publications has led us to a conclusion that intermixing of different metals on an atomic level is ensured by the processes of dry friction and shear deformation of milled particles [14,15]. New experimental evidences are needed in order to elucidate a nature of the process of mechanically-assisted intermixture. In this work, we studied experimentally using X-ray diffraction analysis the dynamics of phase formation in medium-entropy alloy CoCrFeNi and high-entropy equiatomic alloys AlCoCrFeNi and CoCrFeMnNi in course of HEBM. A reason to study four-component alloy is not only the fact that it forms a “core” for other alloys, but also improved properties of this alloy, comparable with those of HEAs [16].

2. Materials and Methods

Commercially available metal powders used as starting materials are listed in Table 1.

Table 1. Characteristics of powders used in experiments (all from Russian manufactures).

| Powder | Purity, % | Particle size, μm | Crystal structure | Atomic radius, \AA [5] |
|--------|-----------|------------------------------|----------------------|---------------------------------|
| Co | >99.35 | <71 | HCP | 1.251 |
| Fe | >99.9 | 10–20 | BCC | 1.241 |
| Ni | >99.5 | ~150 | FCC | 1.246 |
| Cr | >98.5 | <125 | BCC | 1.249 |
| Al | 99.7 | 10 (mean) | FCC | 1.432 |
| Mn | >99.7 | <400 | α -Mn (cubic) | 1.350 |

The powders were blended in equimolar proportions and mechanically alloyed by HEBM in a water-cooled ball mill AGO-2 (Novosibirsk, Russia). The powder mixture (10 g) was placed in a steel jar (volume 160 cm³) filled with atmospheric air at normal conditions, together with milling steel balls, then the jar was hermetically closed. Amount of gaseous oxygen that remains inside the jar (about 0.04 g) is too small and cannot notably oxidize the metals or affect alloy composition. This question was considered elsewhere [10,15]. The diameter of steel balls was 9 mm; the ball-to-powder mass ratio was

20 : 1 in all experiments. The mill rotating speed of the AGO-2 was equal to 912 rpm, which corresponded to 2220 rpm for jars.

Crystal structure and phase analysis was made by means of X-ray diffraction methods, using a DRON-3M diffractometer (Russia). As a rule, Fe- $K\alpha$ radiation ($\lambda = 0.19374$ nm) was used for the sake of better angular resolution and peak/background ratio. XRD patterns were scanned from 34° to 90° (2θ) in a step-by-step scanning mode with a scan increment of 0.02° . The exposure time was 2 s. Fitting the XRD peaks was made using NPP Burevestnik software Data Processing DrWin (registration number 2010617752 on 23.11.10, Russia) that was developed for DRON diffractometers (<https://bourestnik.com/production/x-ray-diffraction-analysis/dron-8/>). Data processing was carried out in two steps. The first step included background approximation by a polynomial of order $n = 3$, peak search, determination of angle positions and heights of peaks. The second step involved the refinement of peak parameters by profile fitting. Profile of each determined diffraction line was approximated by a doublet of asymmetric pseudo-Voigt functions. Silicon (NIST SRM 640b brand) was used as an internal reference in precise measurements of unit cell parameters. An example of the XRD pattern treatment is presented in supplementary files, Fig. S1.

The SEM and EDS analyses were made using a LEO 1450 VP microscope (Carl Zeiss, Germany) equipped with an energy-dispersive X-ray spectrometer INCA 300. An average composition was detected by EDS analysis of the 16×12 μm area on the cross-section. In order to estimate homogeneity of microstructure and scattering of local compositions, numerous EDS analyses were made in random points on the surface of cross-section. In case of strong scattering, 16 points were tested for each sample; this number decreased to 5–6 points in case of uniform samples with minor fluctuations of local composition. Vickers microhardness (HV) was measured with a PMT3 tester (Russia) under a 50-g load. Local EDS analysis and microhardness measurements were made within alloy particles stacked at the surface of milling balls, while the XRD analysis was made using powders remaining free inside the jar. It was shown earlier that the sticking and separation of the powder particles occurs periodically during the HEBM of metallic mixtures, so that the stuck and separate particles had similar microstructure and chemical composition [15]. The balls, together with the stuck layers of alloy particles, were cut using diamond saw, and their cross sections were mechanically polished for use in SEM, EDS, and HV studies.

3. Results

The transformations of crystal structure and microstructure in the four-component Co-Cr-Fe-Ni system are presented in Figs. 1 and 2. A specific abrupt shifting and narrowing of the main XRD peak were observed after 20 min of HEBM (see arrows in Fig. 1). According to SEM results, a complete homogenization of microstructure was achieved after 30 min of milling (Fig. 2). An averaged chemical composition as determined by EDS from the rectangular area 16×12 μm remained almost constant after

20 min of HEBM (Table 2). Minor excess of Fe and Cr can appear probably due to abrasive wear of milling balls and jars.

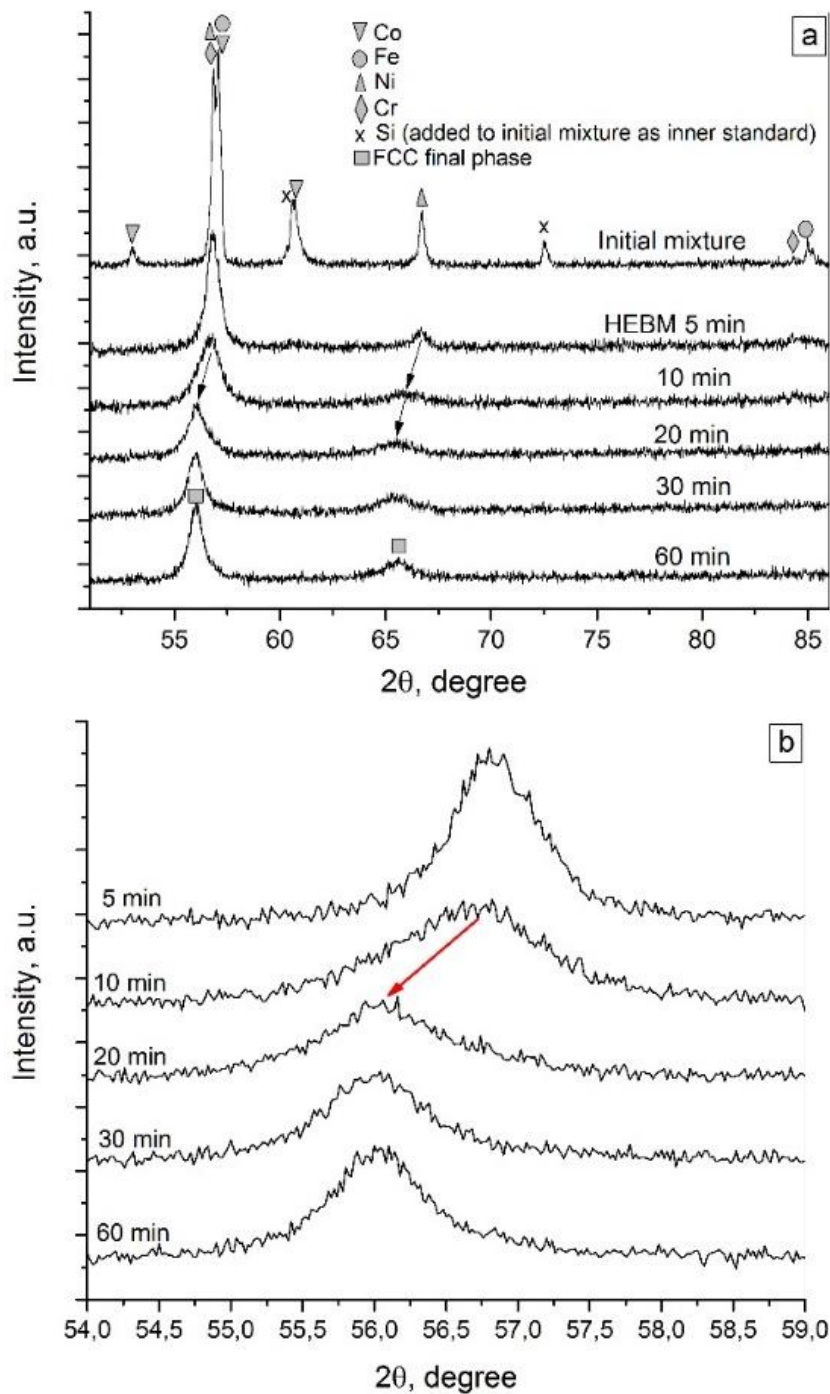


Fig. 1. XRD patterns of the equiatomic CoCrFeNi alloy in course of HEBM: overall view (a) and the expanded 100% peak (b). For the initial mixture see also Fig.S2 in the supplementary file.

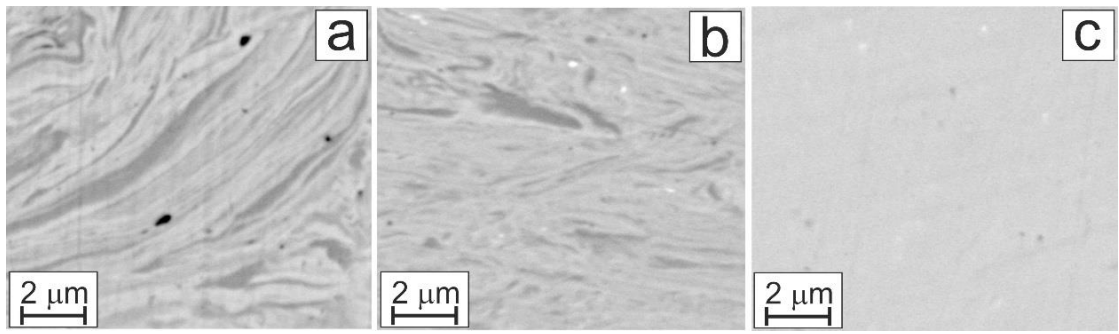


Fig. 2. SEM images of the CoCrFeNi alloy after different time of HEBM: 5 min (a), 10 min (b), and 30 min (c).

Table 2

EDS results for averaged composition of the quaternary alloy (scanning area $16 \times 12 \mu\text{m}$).

| HEBM time, min | Concentration (at. %) of the components averaged over $16 \times 12 \mu\text{m}$ area | | | |
|-------------------|------------------------------------------------------------------------------------------|-------|-------|-------|
| | Co | Cr | Fe | Ni |
| 20 | 24.76 | 25.00 | 26.51 | 23.72 |
| 30 | 24.23 | 25.47 | 25.68 | 24.61 |
| 60 | 24.24 | 25.71 | 26.40 | 23.65 |

Local EDS micro-analysis of the samples taken after different time of HEBM (analysis in random points on cross-sections) shows that a large spread of concentrations exists during the first 5–20 min of HEBM (Fig. 3a-d). The largest scattering of concentration can be observed for Cr: Cr-rich inclusions were detected at longer milling times (Fig. 3d). The delay of Cr dissolution in the multicomponent phase can be associated with higher hardness and lower ductility of chromium particles compared to those of Ni, Co, and Fe. Nevertheless, all experimental points gather together after 60 min of HEBM, which indicated formation of single homogeneous solid solution.

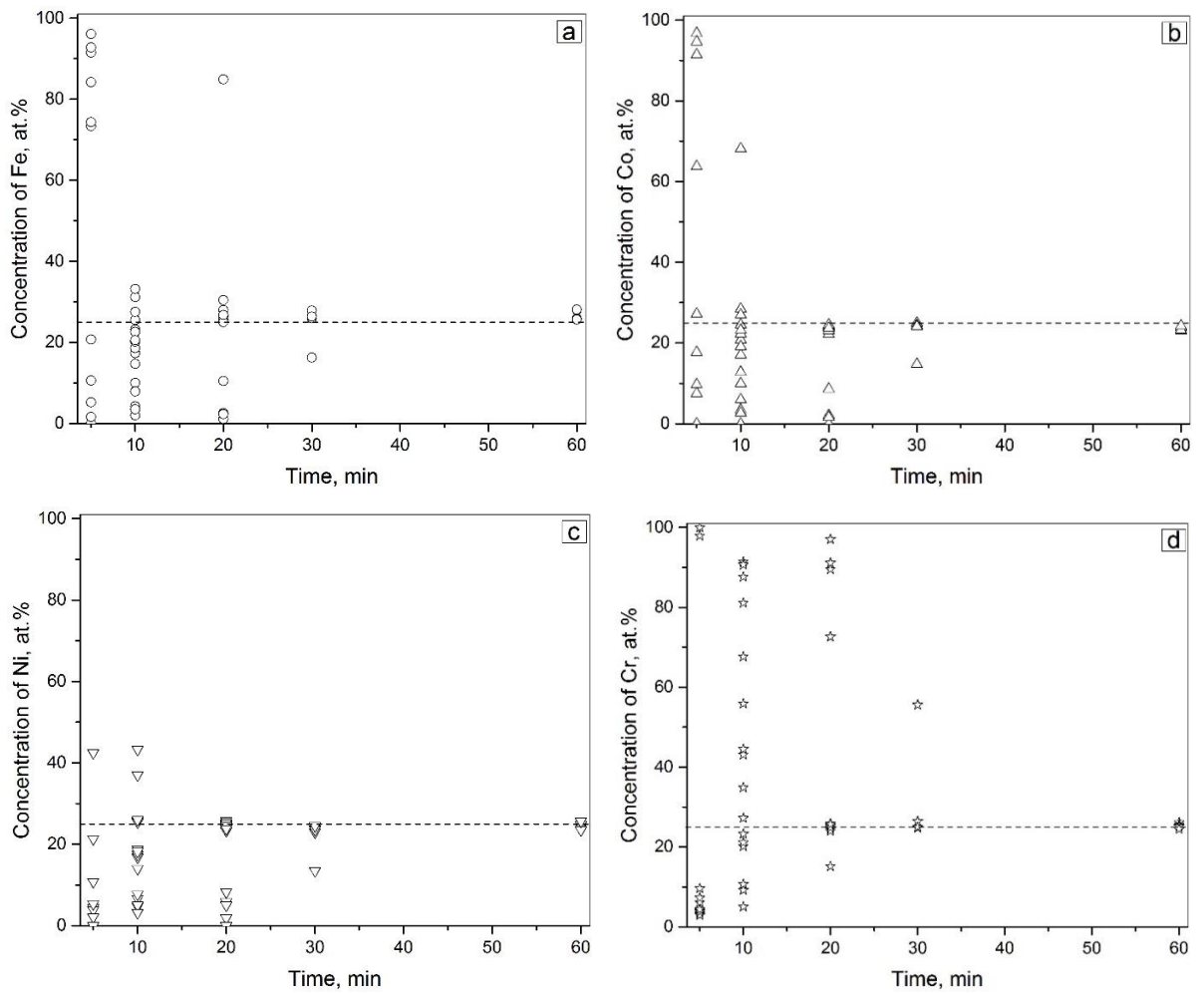


Fig. 3. EDS results for concentration of the elements at random points over the cross-section of CoCrFeNi powder as a function of HEBM time for Fe (a), Co (b), Ni (c), and Cr (d).

Microhardness of the alloy particles slightly increases during the first 20 min of HEBM and then levels-off (Fig. 4). Large spread in HV values, remaining even after 60 min HEBM, indicates that the extent of local cold-working markedly changes across the alloy particles. During the first 20 min of HEBM, variation in microhardness can be attributed to fluctuations of chemical composition inside the powder particles (Fig. 2, Fig. 3). However, the notable spreading of the HV values persists after 60 min of HEBM, when the chemical composition is uniform. This indicates that the as-milled multicomponent alloy undergoes fluctuations of local microhardness that can be related to various extents of plastic deformation and cold-working in different areas of the powder particles or in different particles. High-temperature treatment of the powder can diminish the scattering of HV values. For example, the alloy CoCrFeNiAl, consolidated by spark plasma synthesis at 1000 °C from the mechanically synthesized powder, showed a hardness of $436 \pm 17 \text{ kg/mm}^2$ [9], i.e. at a standard deviation of below 4%.

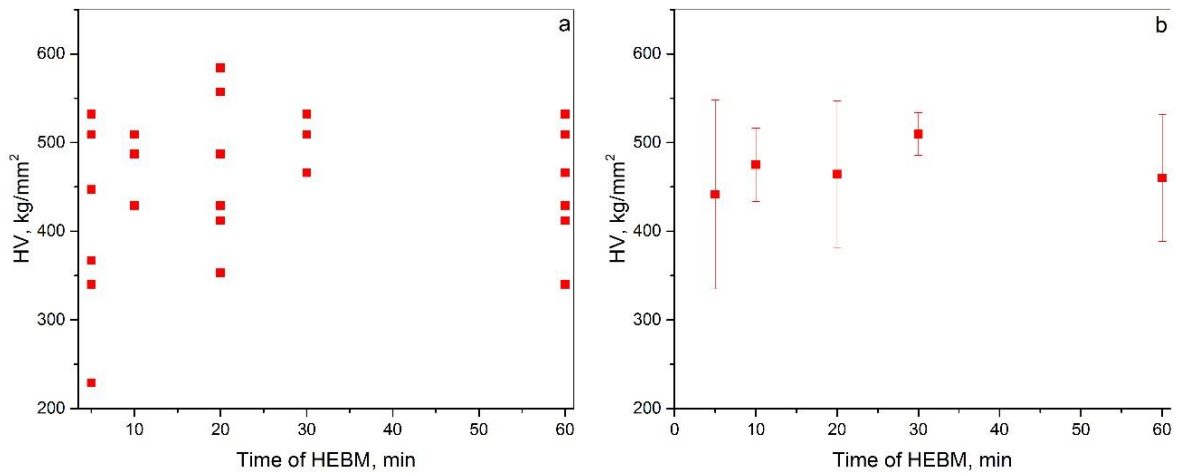


Fig. 4. Microhardness HV for CoCrFeNi powders as a function of HEBM time (AGO-2): data points (a) and their mean values with standard deviations (b).

Dynamics of the major XRD peak transformations in equimolar 5-component high-entropy systems is shown in Fig. 5. The abovementioned characteristic jump of the XRD peaks was observed between 60 and 90 min HEBM in the Co–Fe–Ni–Cr–Mn and Co–Fe–Ni–Cr–Al systems (Fig. 5a,b). For the sake of obviousness of this effect, the small angular range in the vicinity of the major (100%) peak is presented in Fig. 5. The complete XRD patterns for these alloys are available in our previous works [10,13].

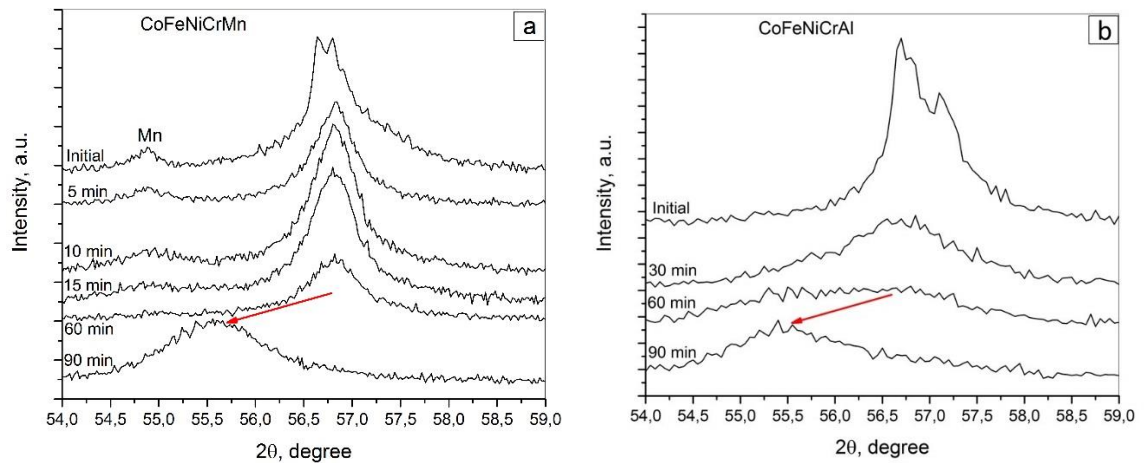


Fig. 5. Evolution of the most intense (100%) XRD peaks during HEBM for some quinary systems: Co–Fe–Ni–Cr–Mn (a), and Co–Fe–Ni–Cr–Al (b).

4. Discussion

Based on the experimental results, we can outline some common features of phase and structural transformations taking place during mechanical alloying of 3d transition metals. Multiple severe plastic deformations of ductile metals, cold welding, and mutual interdiffusion during HEBM result in

broadening XRD peaks, which can be attributed to a decrease in crystallite size, an increase in concentration of lattice defects and grain boundaries.

A large width of XRD peaks formed during HEBM makes difficult precise measurement of cell parameters, so that we could only roughly estimate d-spacing from position of the strongest peaks (Fig. 6). A difference between interplanar spacings for close-packed atomic planes in pure metals is about 1% or less, as is indicated by bars at zero time (before HEBM) in Fig. 6. After 5-min HEBM, the fused peaks form, and the difference between d-spacing for four-, and five-component alloys is below 0.5%. A delay time before the mentioned specific jump of the XRD peak, which means a sudden increase in d-spacing, increases on going from four-component system to five-component alloys. After the transformation, d-spacing increases by about 1.5% in quaternary systems and by about 2.5% in quinary systems.

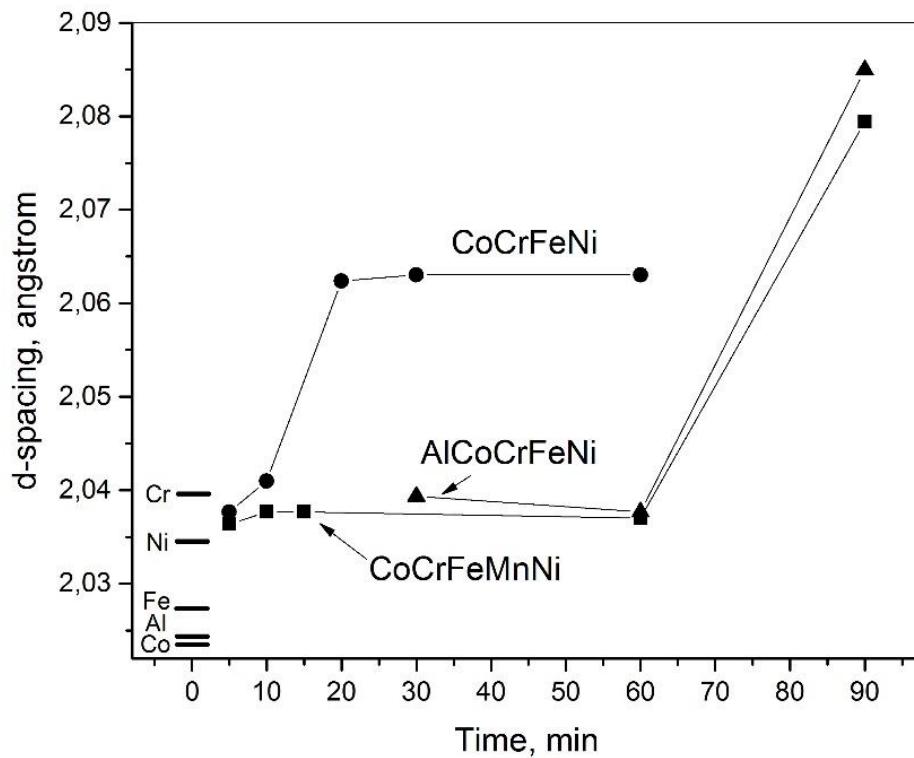


Fig. 6. Evolution of interplanar distance (d-spacing) in the course of HEBM as evaluated from position of the strongest XRD peak.

Assuming that broadening of XRD peaks in course of HEBM indicates decreasing of crystalline size, we can estimate crystalline size (d) using Scherrer formula

$$d = \frac{K\lambda}{\beta \cos(\theta)},$$

where $\lambda = 0.19374$ nm is the wavelength of probing X-rays used in this work (Fe- K_{α}); β is half-width of the diffraction peak (the most intense 100 % peaks were measured); θ is angular peak position, K is a dimensionless coefficient close to unity and defined by a shape of crystallites (we used spherical approximation with $K \approx 0.9$). The results of calculations are presented in Table 3. It must be underscored that these values do not consider fine effects (such as microstress, hardware broadening or concentrations of dislocations), therefore, the Table presents quite rough approximation. Nevertheless, the effects of sudden peak shifting occurring after some critical time of HEBM and changing of the peaks with simultaneously with the shifting, are quite evident.

Table 3

Size of crystallites before and after formation of final phase in the course of HEBM as estimated from half-width of the most intense (100%) diffraction peak.

| System | Crystallite size d before peak shifting during HEBM, nm | Crystalline size d after peak shifting during HEBM, nm |
|------------|-----------------------------------------------------------|----------------------------------------------------------|
| CoFeNiCr | 9.8 | 13.5 |
| CoFeNiCrMn | 17.8 | 10.7 |
| CoFeNiCrAl | 4.4 | 7.8 |

In the quaternary system, peak broadening suggests that crystallite size decreases down to ~ 10 nm after 10 min of HEBM. When peak jump happens and the single FCC phase forms, the width of the XRD peak decreases simultaneously with the drift of its position, thus indicating a growth in crystallite size up to 13–14 nm. We can surmise that crystalline grains of the FCC phase nucleate and grow in a very fine-grained polycrystalline matrix formed due to multiple severe plastic deformation of individual metal crystallites. A similar behavior was observed for the CoFeNiCrAl HEA, where crystallite size grew from 4.4 to 7.8 nm. However, in the CoFeNiCrMn system the formation of FCC phase led to a decrease in the mean crystallite size (further broadening of XRD peaks).

A chemical micro-heterogeneity, that manifests itself in the SEM images taken during the first 5–10 min of HEBM (Fig. 2a,b), can also affect the width of XRD peaks. As is known, the composite particles with specific lamellar microstructure can form in the very beginning of HEBM of dissimilar metals. Such microstructures were first observed for binary mixtures such as Fe–Al or Ni–Al [17,18] and then other numerous multicomponent metallic systems [7–10,13,14,19–21]. At the same time, the XRD results (Fig. 1) show virtually the “single phase” patterns with broad peaks after 5 and 10 min of HEBM. The half-width of the 111 and 200 peaks after 10 min of HEBM is about 1–2 deg, which is large enough to include two or more overlapped peaks of different phases (solid solutions) inside one broad peak. Therefore, chemically micro-heterogeneous alloy may have a simple XRD pattern with broad

peaks, and only results of the SEM and local EDS (Fig. 2 and Fig. 3) provide the reliable data concerning the homogenization of local chemical composition.

Thus, we can suggest the following mechanism of synthesis of medium- and high-entropy alloys by HEBM. In the beginning, intense plastic deformation results in formation of different solid solutions on the base of Fe, Ni, Co, etc., and decreasing crystalline size of all these phases. This stage is characterized by significant variations in local chemical concentrations and broadening of XRD peaks. As a result, the most intense XRD peaks of individual metals and solid solutions, that were close to each other for the considering systems, fuse together to form one broad major peak. The minor peaks diminished due to broadening. When the crystallite size achieves some critical level (about 10 nm or less), relatively fast recrystallization with phase transformation happens, which results in the formation of single multicomponent phase. All intermediate solid solutions formed on the base of Fe, Ni, or Co crystal structures convert into this phase. Such transformation manifests itself as the sudden peak shifting accompanied with changing of the peak with.

5. Conclusions

We have studied dynamics and mechanism of mechanical synthesis of medium- and high-entropy alloys on the base of 3-d transition metals. Results allow the following conclusions.

The mechanical synthesis of multicomponent alloy occurs in two stages:

- a) At the first stage, refinement of crystallites and accumulation of crystal structure defects take place due to severe plastic deformation and friction of metal particles that induce abnormally fast diffusive intermixing of different metallic atoms. This process results in formation of nanocrystalline intermedium alloy(s) with a crystallite size of about 10 nm.
- b) At the second stage, recrystallization occurs, which leads to the nucleation and growth of multicomponent phase(s) with a simple FCC or BCC structure.

These results can be used to find an optimal route for time-consuming and facile mechanical synthesis of high-entropy alloys.

CRediT authorship contribution statement

Alexander Rogachev: Conceptualization, Writing - original draft, Writing - Review & Editing, Project administration, Resources. **Dmitry Kovalev:** Investigation, Data curation. **Adrien Fourmont:** Methodology, Investigation. **Sergei Vadchenko:** Methodology, Investigation, Data curation. **Nikolas Kochetov:** Methodology, Investigation. **Natalia Shkodich:** Methodology, Investigation, Writing - Review & Editing. **Florence Baras:** Conceptualization, Writing - Review & Editing. **Olivier Politano:** Conceptualization, Writing - Review & Editing. **Dmitry Moskovskikh:** Resources, Writing - Review & Editing

Declaration of competing interest

The authors declare that they have no known competing financial interests or personal relationships that could have appeared to influence the work reported in this paper.

Acknowledgments

Authors acknowledge funding from the Russian Science Foundation (project no. 20-13-00277). We are grateful to Dr. Yu. Scheck for fruitful discussions, Mrs. N. Mukhina for SEM/EDS measurement, and Mrs. A. Belikova for HV measurements.

References

- [1] B. Cantor, I.T.H. Chang, P. Knight, A.J.B. Vincent, Microstructural development in equiatomic multicomponent alloys, *Mater. Sci. Eng. A*. 375–377 (2004) 213–218.
<https://doi.org/10.1016/j.msea.2003.10.257>.
- [2] J.-W. Yeh, S.-K. Chen, S.-J. Lin, J.-Y. Gan, T.-S. Chin, T.-T. Shun, C.-H. Tsau, S.-Y. Chang, Nanostructured High-Entropy Alloys with Multiple Principal Elements: Novel Alloy Design Concepts and Outcomes, *Adv. Eng. Mater.* 6 (2004) 299–303.
<https://doi.org/10.1002/adem.200300567>.
- [3] D.B. Miracle, High entropy alloys as a bold step forward in alloy development, *Nat. Commun.* 10 (2019) 1805. <https://doi.org/10.1038/s41467-019-09700-1>.
- [4] Y. Zhang, T.T. Zuo, Z. Tang, M.C. Gao, K.A. Dahmen, P.K. Liaw, Z.P. Lu, Microstructures and properties of high-entropy alloys, *Prog. Mater. Sci.* 61 (2014) 1–93.
<https://doi.org/10.1016/j.pmatsci.2013.10.001>.
- [5] D.B. Miracle, O.N. Senkov, A critical review of high entropy alloys and related concepts, *Acta Mater.* 122 (2017) 448–511. <https://doi.org/10.1016/j.actamat.2016.08.081>.
- [6] A.S. Rogachev, Structure, Stability, and Properties of High-Entropy Alloys, *Phys. Met. Metallogr.* 121 (2020) 733–764. <https://doi.org/10.1134/S0031918X20080098>.
- [7] K.B. Zhang, Z.Y. Fu, J.Y. Zhang, J. Shi, W.M. Wang, H. Wang, Y.C. Wang, Q.J. Zhang, Nanocrystalline CoCrFeNiCuAl high-entropy solid solution synthesized by mechanical alloying, *J. Alloys Compd.* 485 (2009) L31–L34. <https://doi.org/10.1016/j.jallcom.2009.05.144>.
- [8] W. Chen, Z. Fu, S. Fang, H. Xiao, D. Zhu, Alloying behavior, microstructure and mechanical properties in a FeNiCrCo_{0.3}Al_{0.7} high entropy alloy, *Mater. Des.* 51 (2013) 854–860.
<https://doi.org/10.1016/j.matdes.2013.04.061>.
- [9] A.S. Rogachev, N.A. Kochetov, A. V. Panteleeva, K. V. Kuskov, D.Y. Kovalev, A.S. Shchukin,

S.G. Vadchenko, Y.B. Scheck, High-Energy Ball Milling and Spark Plasma Sintering of the CoCrFeNiAl High-Entropy Alloy, *Metals (Basel)*. 10 (2020) 1489.

<https://doi.org/10.3390/met10111489>.

- [10] A.S. Rogachev, D.Y. Kovalev, N.A. Kochetov, A.S. Shchukin, S.G. Vadchenko, Evolution of crystal structure in high-entropy AlCoCrFeNi alloy: An in situ high-temperature X-ray diffraction study, *J. Alloys Compd.* 861 (2021) 158562.
<https://doi.org/10.1016/j.jallcom.2020.158562>.
- [11] W. Ji, W. Wang, H. Wang, J. Zhang, Y. Wang, F. Zhang, Z. Fu, Alloying behavior and novel properties of CoCrFeNiMn high-entropy alloy fabricated by mechanical alloying and spark plasma sintering, *Intermetallics*. 56 (2015) 24–27.
<https://doi.org/10.1016/j.intermet.2014.08.008>.
- [12] F. Průša, A. Šenková, V. Kučera, J. Čapek, D. Vojtěch, Properties of a high-strength ultrafine-grained CoCrFeNiMn high-entropy alloy prepared by short-term mechanical alloying and spark plasma sintering, *Mater. Sci. Eng. A*. 734 (2018) 341–352.
<https://doi.org/10.1016/j.msea.2018.08.014>.
- [13] A.S. Rogachev, S.G. Vadchenko, N.A. Kochetov, S. Rouvimov, D.Y. Kovalev, A.S. Shchukin, D.O. Moskovskikh, A.A. Nepapushev, A.S. Mukasyan, Structure and properties of equiatomic CoCrFeNiMn alloy fabricated by high-energy ball milling and spark plasma sintering, *J. Alloys Compd.* 805 (2019) 1237–1245. <https://doi.org/10.1016/j.jallcom.2019.07.195>.
- [14] A.S. Rogachev, N.F. Shkodich, S.G. Vadchenko, F. Baras, D.Y. Kovalev, S. Rouvimov, A.A. Nepapushev, A.S. Mukasyan, Influence of the high energy ball milling on structure and reactivity of the Ni + Al powder mixture, *J. Alloys Compd.* 577 (2013) 600–605.
- [15] A.S. Rogachev, Mechanical activation of heterogeneous exothermic reactions in powder mixtures, *Russ. Chem. Rev.* 88 (2019) 875–900. <https://doi.org/10.1070/RCR4884>.
- [16] J. Xu, X. Kong, M. Chen, Q. Wang, F. Wang, High-entropy FeNiCoCr alloys with improved mechanical and tribological properties by tailoring composition and controlling oxidation, *J. Mater. Sci. Technol.* 82 (2021) 207–213. <https://doi.org/10.1016/j.jmst.2020.12.042>.
- [17] F. Bernard, E. Gaffet, Mechanical alloying in the SHS research, *Int. J. Self-Propagating High-Temperature Synth.* 10 (2001) 109–132.
- [18] A.S. Rogachev, N.A. Kochetov, V. V. Kurbatkina, E.A. Levashov, P.S. Grinchuk, O.S. Rabinovich, N. V. Sachkova, F. Bernard, Microstructural aspects of gasless combustion of mechanically activated mixtures, *Combust. Explos. Shock Waves*. 42 (2006) 421–429.
- [19] C.K. Lin, S.W. Liu, P.Y. Lee, Preparation and thermal stability of Zr-Ti-Al-Ni-Cu amorphous powders by mechanical alloying technique, *Metall. Mater. Trans. A*. 32 (2001) 1777–1786.
<https://doi.org/10.1007/s11661-001-0154-2>.

- [20] Y.-L. Chen, Y.-H. Hu, C.-W. Tsai, C.-A. Hsieh, S.-W. Kao, J.-W. Yeh, T.-S. Chin, S.-K. Chen, Alloying behavior of binary to octonary alloys based on Cu–Ni–Al–Co–Cr–Fe–Ti–Mo during mechanical alloying, *J. Alloys Compd.* 477 (2009) 696–705. <https://doi.org/10.1016/j.jallcom.2008.10.111>.
- [21] Y.-L. Chen, Y.-H. Hu, C.-A. Hsieh, J.-W. Yeh, S.-K. Chen, Competition between elements during mechanical alloying in an octonary multi-principal-element alloy system, *J. Alloys Compd.* 481 (2009) 768–775. <https://doi.org/10.1016/j.jallcom.2009.03.087>.